

Physical properties of the very heavy fermion YbCu₄Ni

J.G. Sereni¹, I. Čurlík², M. Giovannini³, A. Strydom^{4,5}, M. Reiffers²

¹*Department of Physics, CAB-CNEA, CONICET, 8400 San Carlos de Bariloche, Argentina*

²*Faculty of Humanities and Natural Sciences, University of Prešov, 17. novembra 1, Prešov, Slovakia*

³*Department of Physics and CNR-SPIN, University of Genova, Via Dodecaneso 31, Genova, Italy*

⁴*Highly Correlated Matter Research Group, Physics Department,*

University of Johannesburg, PO Box 524, Auckland Park 2006, South Africa

⁵*Max Planck Institute for Chemical Physics of Solids, Nthnitzerstr.40, D-01187 Dresden, Germany.*

(Dated: May 22, 2018)

The physical properties of the very heavy fermion YbCu₄Ni were characterized through structural, magnetic, thermal and transport studies along nearly four decades of temperature ranging between 50 milikelvin and 300 K. At high temperature, the crystal electric field levels splitting was determined with $\Delta_1(\Gamma_6) = 85$ K and $\Delta_2(\Gamma_8) \approx 200$ K, the latter being a quartet in this cubic symmetry. An effective magnetic moment $\mu_{eff} \approx 3\mu_B$ is evaluated for the Γ_7 ground state, while at high temperature the value for a Yb³⁺ ion is observed. At low temperature this compounds shows the typical behavior of a magnetically frustrated system undergoing a change of regime at a characteristic temperature $T^* \approx 200$ mK into a sort of Fermi-liquid type 'plateau' of the specific heat: $C_m/T|_{T \rightarrow 0} = \text{const}$. The change in the temperature dependence of the specific heat coincides with a maximum and a discontinuity in respective inductive and dissipative components of the ac-susceptibility. More details from the nature of this ground state are revealed by the specific heat behavior under applied magnetic field.

I. INTRODUCTION

There is an increasing number of new Yb-based compounds which do not show long range magnetic order down to the milikelvin range of temperature. Since they are characterized by having robust magnetic moments and by exhibiting a divergent increase of magnetic correlations in their paramagnetic phase upon cooling [1], it is expected that they belong to a different class of materials than those placed around a quantum critical point [2]. The strong increase of the density of magnetic excitations is reflected in power law dependencies of the specific heat: $C_m(T)/T \propto 1/T^Q$, with exponents ranging between $1 < Q \leq 2$ that clearly exceed the $C_m/T|_{T \rightarrow 0}$ values of usual non-fermi-liquids (NFL) [3] that increase as a $-\ln(T/T_0)$ with decreasing temperature. These compounds can be called very-heavy fermions (VHF) because their $C_m/T|_{T \rightarrow 0}$ range between ≈ 5 and ≈ 12 J/molK² [4].

Two scenarios were proposed for the lack of long range magnetic order in these compounds, one due to a very weak magnetic interaction between Yb ions and the other to magnetic frustration. The former applies to YbPt₂In and YbPt₂Sn compounds that show the record high ≈ 12 J/molK² value [5] after undergoing a maximum of $C_m(T)/T$ around 250 mK. Magnetic frustration can be originated by peculiar geometric coordination of the magnetic moments [6] or by the competition between magnetic interactions of different nature. Triangular (2D) or tetrahedral (3D) are the typical atomic configurations producing frustration at low temperature, with the striking feature that a number of Yb systems show a coincident plateau of $C_m/T|_{T \rightarrow 0} = 7 \pm 0.5$ J/molK² below a deviation from

their power law dependence of $C_m/T(T)$ within the mK range [4] at a characteristic temperature T^* .

The mentioned absence of magnetic order in these VHF was verified by different type of measurements besides specific heat. For example, electrical resistivity (ρ) of YbCu_{5-x}Au_x [1] and PrInAg₂ [8] decreases continuously with temperature around T^* without showing any discontinuity in their thermal slopes after undergoing a broad maximum. The lack of magnetic order in YbCu_{5-x}Au_x down to 0.02 K was confirmed through NQR and μ SR measurements [9].

A relevant aspect of the VHF compounds concerns their potential application for adiabatic demagnetization refrigeration based upon the large amount of entropy accumulated below 1 K that can be removed under magnetic field. This property was properly explored in at least two compounds: YbPt₂In [10] and (Yb_{1-x}Sc_x)Co₂Zn₂₀ [11]. The latter YbCo₂Zn₂₀ [12] together with YbBiPt [13] belong to the mentioned class of compounds showing similar $C_m/T|_{T \rightarrow 0} \approx 7$ J/molK² value below T^* . After having recognized the YbCu_{5-x}Au_x ($0.4 \leq x \leq 0.7$) family as belonging to this "plateau" type group while the stoichiometric compound YbCu₄Au presents a cusp at $T \approx 0.8$ K [14], we have searched for an alternative composition in order to identify the main property producing such a different behavior. With this aim we have studied the physical properties of the isotopic compound YbCu₄Ni, where nearly isochoric Ni atoms with $\approx 3\%$ smaller metallic radius than Cu, instead of Au that is $\approx 20\%$ larger.

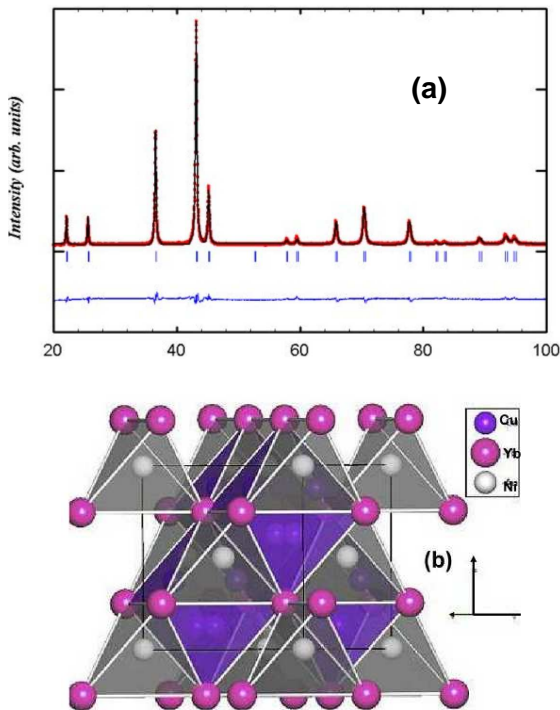


FIG. 1. a) The experimental x-ray diffraction powder pattern of YbCu_4Ni compared with the calculated diffraction diagram. The experimental data are shown by symbols, whereas the line through the data represents the results of the Rietveld refinement. The lower curve is the difference curve. The ticks indicate Bragg peak positions. b) Crystal structure seen as edge-sharing tetrahedra with Yb ions located at the vertices (unit cell indicated by black lines) after [15].

II. EXPERIMENTAL DETAILS

The polycrystalline samples of YbCu_4Ni and LuCu_4Ni were prepared after weighing stoichiometric amounts of the elements with the following nominal purity Yb-99.9% mass, Lu-99.9% mass, Cu-99.999% mass and Ni-99.995% mass. Then the elements were enclosed in small tantalum crucibles and sealed by arc welding under pure argon. The samples were melted in an induction furnace under a stream of pure argon. To ensure homogeneity during the melting, the crucibles were continuously shaken. The samples were then annealed in a resistive furnace for two weeks at 700 C and finally quenched in cold water.

The two samples YbCu_4Ni and LuCu_4Ni were characterized by optical and electron microscopy and by quantitative electron probe microanalysis. The crys-

TABLE I. Structural parameters of YbCu_4Ni refined from x-ray data in the space group $F-43m$. Residual values: $R_B = 4.10\%$, $R_F = 5.58\%$, $R_{WP} = 6.86\%$.

Atom	Site	x	y	z
Yb	4c	0.25	0.25	0.25
Cu	16c	0.6259(1)	0.6259(1)	0.6259(1)
Ni	4c	0	0	0

tal structure was examined by x-ray diffraction (XRD) using a $K\alpha$ radiation. Rietveld matrix full profile refinements were performed using the program FULLPROF [16].

Specific heat measurements on YbCu_4Ni were carried out in a commercial PPMS equipment within the temperature range $0.4 < T < 300$ K, in zero and applied magnetic fields up to 9 T. Using the same device the temperature dependence of electrical resistivity was measured within the mentioned ranges of temperature and field for magnetoresistance. The low temperature resistivity measurements ($50 \text{ mK} < T < 4 \text{ K}$) were performed using a four-coils configuration, applying an AC current of 0.2 mA with a $f = 18.3$ Hz frequency. The temperature dependence of magnetization and magnetic susceptibility were obtained using commercial MPMS. At low temperature (between 50 mK and 4 K) AC-magnetic susceptibility was measured applying an excitation intensity of 1 Oe using different frequencies: $f = 4, 1$ and 0.1 kHz.

III. EXPERIMENTAL RESULTS

A. Crystal structure of YbCu_4Ni

Single-phase sample material of YbCu_4Ni was obtained showing a face-centered cubic (FCC) structure of MgCu_4Sn type (ternary derivative of the AuBe_5) with lattice constant: $a = 6.943 \text{ \AA}$. The structural results of the Rietveld profile fitting are summarized in Table I and the corresponding diffraction pattern is shown in Fig. 1a. The structure was checked with respect to ordered or disordered locations of atoms in the structure, but the compound resulted to be a fully ordered compound with a full occupation of the atoms in each site. As depicted in Fig. 1b, this FCC lattice can be viewed as a network of edge-sharing tetrahedra with Yb magnetic ions located at the vertices [15] being a 3D analogue of a triangular lattice. The details of the structural refinement for the isotopic LuCu_4Ni compound were reported in a previous work [17].

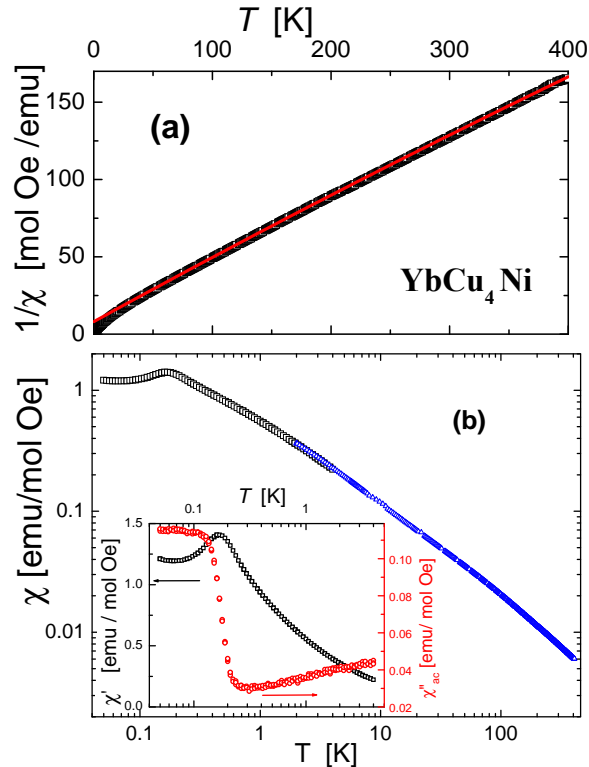


FIG. 2. a) High temperature dependence of the inverse magnetic susceptibility, b) low temperature inductive component of AC-susceptibility scaled with high temperature DC-susceptibility in a double logarithmic representation. Inset: inductive (χ' , left axis) and dissipative (χ'' , right axis) components of AC susceptibility in a semi-logarithmic representation.

B. Magnetic susceptibility and magnetization

In Fig. 2a the inverse magnetic susceptibility ($1/\chi$) of YbCu_4Ni is shown between 2 and 400 K. This temperature dependence can be described by a simple Curie-Weiss law with a negligible Pauli-type contribution ($\chi_0 = 4 \times 10^{-4}$ emu/mol Oe): $\chi(T) = C_c/(T + \theta_P) + \chi_0$. The Curie constant (C_c) extracted from a fit on the high temperature range: 70 - 300 K, reveals an effective magnetic moment $\mu_{eff} = 4.42\mu_B$, close to the free Yb^{3+} ion value. The paramagnetic Curie-Weiss temperature $\theta_P = -19$ K indicates a dominating antiferromagnetic exchange at high temperature and a weak Kondo effect affecting the excited crystal electric field (CEF) levels. Below $T = 70$ K, $1/\chi$ turns down due to a smaller μ_{eff} value of the ground state (GS), which between $5 \geq T \geq 2$ K is evaluated as $\mu_{eff}^{GS} \approx 3.1\mu_B$ with a weak intensity of the molecular field $\theta_P^{GS} = -1.3$ K.

Below 4 K the magnetic susceptibility was measured

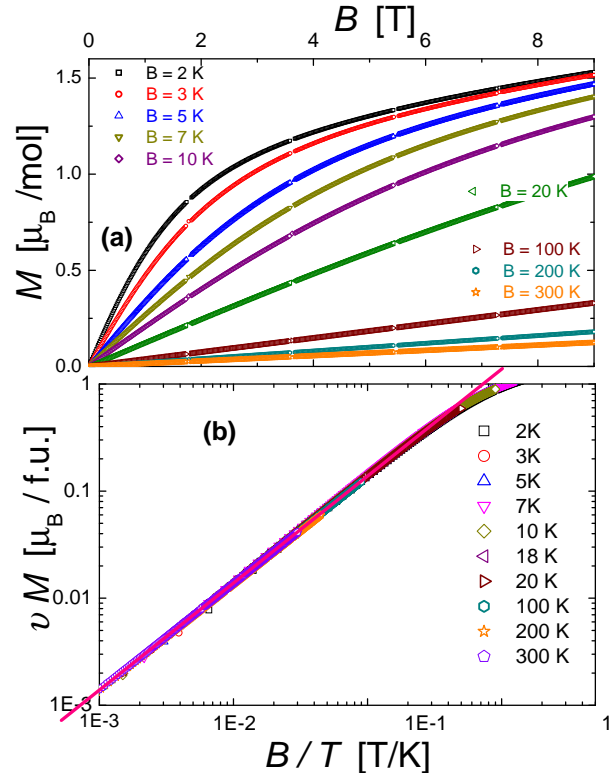


FIG. 3. (a) Scaled magnetization measurements versus field up to 9 T performed between 2 K and room temperature. (b) Collapsed curves scaling with $x = B/T$ and $y = \nu \times M$, with ν accounting for the CEF progressive thermal occupation. Notice the double logarithmic scale.

by an AC- method down to 50 mK, without detecting a frequency dependence, see the inset in Fig. 2b. The results for $f = 4$ kHz show a maximum in the inductive component $\chi'(T)$ at $T_{max}^{\chi} \approx 170$ mK and a clear step in the dissipative component (χ'') at the same temperature. This feature will be discussed in the following section together with the onset of coherence in $\rho(T)$ and the $C_m(T)/T|_{T \rightarrow 0}$ plateau. The low temperature $\chi'(T)$ dependence is overlapped with the high temperature χ_{DC} in Fig. 2b within 2 to 4 K, using the coincident thermal slope as a matching criterion, notice the double logarithmic representation.

The magnetization measurements performed between 2 K and room temperature applying magnetic field up to 9 T are presented in Fig. 3a. Since this system does not show magnetic order it is interesting to recognize up to what extent it can be considered a standard paramagnet (e.g. Curie-Weiss type) at low temperature. The strong curvature observed in Fig. 3a at $T = 2$ K raises the question whether it is due to the effect of an emerging very low temperature interaction or it corresponds to the typical curvature of a Brillouin function $B_J(x)$, with $x = B/T$. For

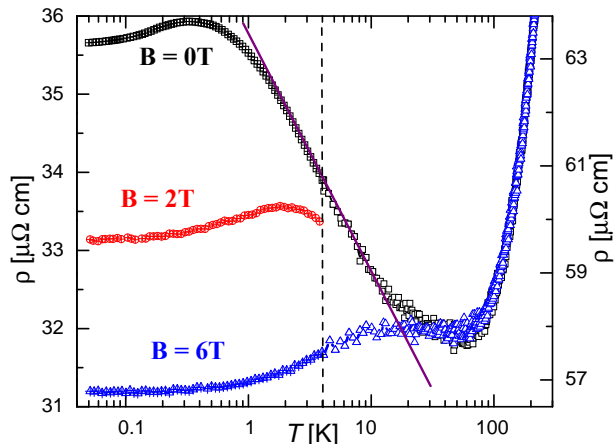


FIG. 4. Logarithmic temperature dependence of the electrical resistivity within four decades of temperature at $B = 0$ and 6 T, measured in different cryostats. Dashed (vertical) line indicates the data matched at $T = 4$ K using a ratio of 1.8 in the form factor (see the text). Straight (purple) line remarks the logarithmic T dependence between $2 < T < 10$ K. The $\rho(T \leq 4, B = 2$ T) K data are included to show the T_{max}^{ρ} variation with field.

this purpose we have scaled all $M(B)$ curves between $2 \leq T \leq 300$ K using $x = B/T$ as abscissa and normalizing the magnetization as M/ν , where ν accounts for progressive thermal (i.e. Boltzmann) occupation of the excited CEF levels. It can be appreciated in Fig. 3b how all curves collapse into a unique curve once these two scaling parameters, which characterize the evolution of a typical Curie-Weiss paramagnetic system, are applied.

C. Electrical resistivity and magnetoresistance

The temperature dependence of the electrical resistivity $\rho(T)$ of YbCu_4Ni is presented in Fig. 4 within four decades of temperature at zero and $B = 6$ T, taking the high temperature data from [18]. Since these results were obtained in different cryostats and from different pieces of the poly-crystalline sample, a ratio 1.8 between respective form factors is observed (compare left low temperature with right high temperature axis in Fig. 4). Such a difference is attributed to a different electrical connectivity between grains within the sample. Between room temperature and $T \approx 60$ K, $\rho(T)$ decreases mostly due to the decreasing phonon contribution. Then, below $T \approx 10$ K, $\rho(T)$ shows a typical $\rho(T) \propto -\ln(T/T_0)$ Kondo increase for the $B=0$ data.

After undergoing a broad maximum, centered at $T_{max}^{\rho} \approx 350$ mK in the $B=0$ data, $\rho_0|_{T \rightarrow 0}$ flattens.

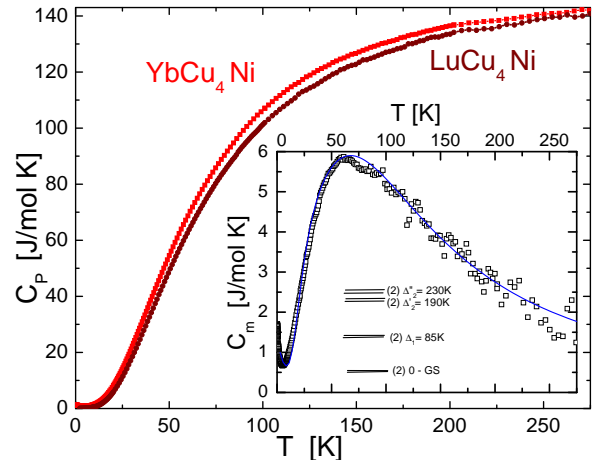


FIG. 5. Specific heat temperature dependencies up to room temperature of YbCu_4Ni and LuCu_4Ni . Inset: high temperature magnetic contribution and a fit accounting for the CEF levels and GS contributions.

Magnetic field induces negative magnetoresistance at low temperature while the T_{max}^{ρ} is shifted to higher temperature. Low temperature $\rho(T \leq 4)$ K data, measured with $B = 2$ T, are included to confirm this field dependent tendency which seems to be proportional to B .

D. Magnetic contribution to the specific heat

Fig. 5 shows the high temperature dependence of the YbCu_4Ni specific heat. Since measured specific heat is usually dominated by electron band (C_{el}), phonon (C_{ph}) and magnetic (C_m) contributions $C_P = C_{el} + C_{ph} + C_m$. In order to subtract the non magnetic components: $C_{el} + C_{ph} = \gamma T + \beta T^3$, we have investigated also the LuCu_4Ni isotype. Its specific heat was also measured within the $0.4 \leq T \leq 300$ K and is included in Fig. 5. Both compounds are close to reach the expected Dulong-Petit values at high temperature. At low temperature, the extracted electron Sommerfeld coefficient for LuCu_4Ni is: $\gamma(\text{Lu}) = 9.5$ mJ/mol K^2 , a typical value for non-magnetic lanthanides compounds. Its Debye temperature: $\theta_D = 325$ K, was computed from the $\beta \approx 0.5$ mJ/mol K^4 coefficient.

At the low temperature limit (i.e. $T < 0.2$ K), the specific heat measurements of YbCu_4Ni show a clear increase attributed to nuclear contribution (C_n). Since this increase is found to proceed as $C_n = A_n/T^2$, in order to compute its contribution we have plot the measured data using a $C_P/T = A_n/T^3 + C_m(T)/T$ temperature dependence. From the fit performed on the studied sample below $T = 0.22$ K one extracts $A_n = 1.35 \cdot 10^{-3}$ JK/mol and $C_m/T|_{T \rightarrow 0} =$

7.5 J/molK². This A_n coefficient is very similar to the one obtained for YbCu_{5-x}Au_x [1] and the value: $C_m/T|_{T \rightarrow 0} = 7.5$ J/molK², places YbCu₄Ni into the class of VHF showing a 'plateau' at $T \rightarrow 0$ [4]. No specific heat jump is observed in $C_m(T)$ rather a well defined cusp at $T_{max}^{C_P} \approx 270$ mK as depicted in Fig. 8.

IV. DISCUSSION

A. Crystal electric field effect

In the inset of Fig. 5 one can see that $C_m(T)$ starts to increase around 10 K once the GS contribution is overcome by that of the excited CEF levels. This Schottky type anomaly, centered at ≈ 60 K, is attributed to the Yb excited crystal electric field CEF levels. In a cubic symmetry, the 8-fold ($N = 2J + 1 = 8$) degenerate ground state given by Hund's rule for a $J = 7/2$ angular momentum splits into two doublets (Γ_6 and Γ_7) and a quartet (Γ_8) according to these calculations of Lea, Leask and Wolf (LLW) [22]. In order to extract the level spectrum, we have fitted the experimental results applying a series of Schottky formulas to account for the contribution of respective excited CEF levels:

$$C_{\text{CEF}}(T) = R \sum_i \left[\frac{\Delta_i}{T} / 2 \cosh\left(\frac{\Delta_i}{2T}\right) \right]^2 \quad (1)$$

being R the gas constant and Δ_i the energy of respective levels.

According to the result, the first excited doublet is located at $\Delta_1 = 90$ K while the second corresponds to the quartet Γ_8 at double the energy: $\Delta_2 \approx 210$ K. Strictly, the fitting curve included in the inset of Fig. 5 also contains the actual GS contribution (see Fig. 6 for more detail) and an improvement obtained by splitting the Γ_8 quartet into two doublets at $\Delta'_2 = 190$ K and $\Delta''_2 = 230$ K. This further splitting mimics an eventual level broadening evaluated around 30 K. This value is in agreement with the observed $\theta_P = -19$ K obtained through an extrapolation from $T \geq 70$ K where the Γ_8 quartet becomes dominant and a Kondo screening effect may be detected. We remark that specific heat results allow to identify the Γ_8 quartet as the most excited level because of its larger degeneracy.

Although the CEF level distribution in YbCu₄Ni has some similarity with that of the isotypic YbCu_{5-x}Au_x, basically because Γ_8 is the upper level [1], the energy distribution of the levels is quite different. This feature can be attributed to the different electronic character between the electron-like Au and the hole-like Ni ligands that presents a point charge of opposite sign among them that clearly modifies the Coulomb potential, though without affecting the local structural symmetry.

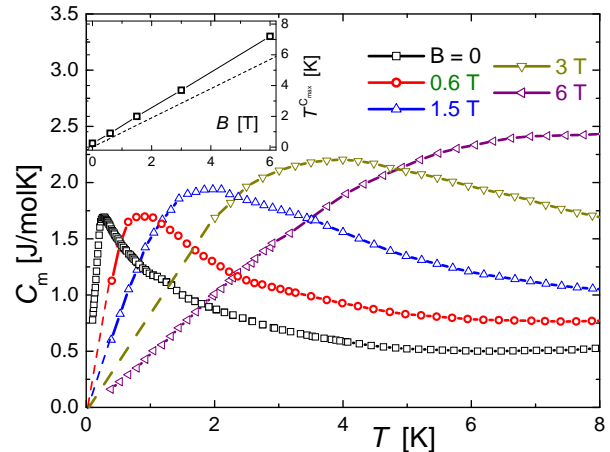


FIG. 6. Low temperature dependencies of the specific heat of YbCu₄Ni under different magnetic fields 0 - 6 T. Inset: Field dependence of the temperature of respective $C_m(T)$ maxima: $T^{C_{max}}$. Dashed line is the computed dependence for the Γ_7 doublet.

B. About the doublet ground state

The same reason that allows to identify the Γ_8 quartet as the most excited level, i.e. its larger degeneracy, impedes to distinguish between the two doublets: Γ_6 and Γ_7 as ground and first excited level. An analysis based on relative degeneracies and levels splitting [19] applied to the LLW tabulations for $J = 7/2$ [22] gives two equivalent possibilities for the LLW parameter: $z = 0.5$ for a Γ_7 -GS and $z = -0.3$ for the corresponding Γ_6 -GS. However, according to previous calculations of the effective moment for those different pseudospin-1/2 doublets [23] $\mu_{eff}(\Gamma_7) = 2.96 \mu_B$ nearly coincides with the experimentally observed value rather than $\mu_{eff}(\Gamma_6) = 2.31 \mu_B$. This result can be checked by computing the expected saturation magnetization: $M_{sat} = g_{eff} J_{eff} \mu_B$. For $g_{eff}(\Gamma_7) = 3.43$ and $J_{eff} = 1/2$ (for the doublet GS), one gets $M_{sat}(\Gamma_7) = 1.72 \mu_B$ which can be expected from the $M(B)$ curve at $T = 2$ K included in Fig. 3a respect to $M_{sat}(\Gamma_6) = 1.33 \mu_B$.

C. Magnetic field effect

The effect of applied magnetic field on the temperature dependence of specific heat, shed further light on the GS nature through the Zeeman splitting dependence on g_{eff} . This field dependence in YbCu₄Ni is presented in Fig. 6 within the $0.4 \leq T \leq 6$ K range and fields up to 9 Tesla. The $C_P(T, B = 0)$ maximum ($T_{max}^{C_P}$) ≈ 270 mK, shifts to higher temperature proportionally to the field intensity as shown in the inset

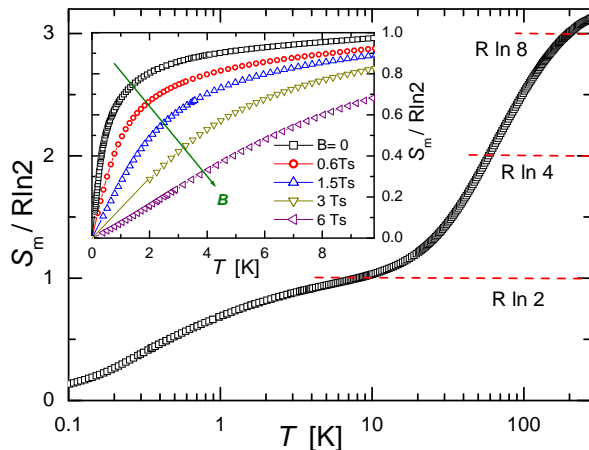


FIG. 7. The temperature dependence of the magnetic entropy of YbCu_4Ni in a logarithmic temperature scale. The inset shows the entropy gain with different applied fields, in linear temperature scale.

of Fig. 6. Despite the fact that $C_P(T, B = 0)$ is better described as a Kondo-like anomaly [20] rather than a Schottky one (see Fig. 6), it is expected that the spin-up and spin-down components split by magnetic field tend to a Schottky anomaly at high enough field, i.e. $\mu B \gg k_B T$ [21]. This criterion, based in the Zeeman splitting of the GS levels, one can confirm its Γ_7 -GS nature applying the $T(C_{m,x}) = 0.42 \times g_{eff} B (\mu_B/k_B)$ relation [24] to obtain the dashed line in the inset of Fig. 6 taking $g_{eff}(\Gamma_7) = 3.43$. Similar magnetic field effects on $C_m(T, B)$ was reported on cubic $\text{Yb}_{0.24}\text{Sn}_{0.76}\text{Ru}$ [23]. In this compound, however, the value of the maximum of $C_m(T)$ is about 35% larger than in the stoichiometric compound studied in this work.

D. Entropy

The magnetic entropy gain (S_m) of YbCu_4Ni along the full range of temperature is displayed in Fig. 7 in a logarithmic temperature scale. It is computed from the magnetic contribution to the specific heat as $S_m = \int C_m/T dT$.

At room temperature, the entropy slightly exceeds the expected value for the 8 fold degenerated $J = 7/2$ Hund's rule GS of Yb^{3+} $S_m = R \ln 8 = 17.28 \text{ J/mol K}$. This excess of entropy is probably due to an under evaluation of the phonon contribution at high temperature. The flattening of $S_m(T)$ around 10 K observed in Fig. 7 corresponds to $S_m = R \ln 2$, indicating that the doublet GS is well separated from the first excited CEF level at $\Delta_1 = 85 \text{ K}$.

At low temperature, the change of curvature ob-

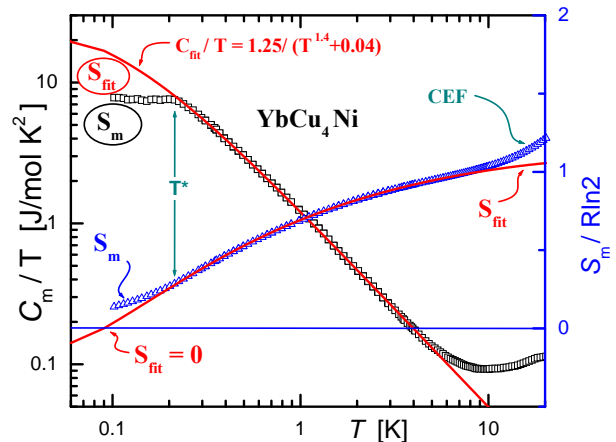


FIG. 8. Comparison between measured $C_m(T)/T$ and fitted $C_{fit}/T|_{T>T^*}$ (continuous curve) dependencies referred to the left axis in double logarithmic representation. On the right axis (linear scale), the temperature dependencies of respective entropies are referred showing how $S_{fit} \rightarrow 0$ at $T > 0$. The value of $S_{fit}(T \rightarrow \infty) = R \ln 2$ is taken as reference for the doublet GS. CEF indicates the onset of excited crystal field levels contribution above about 3 K.

served below $T \approx 300 \text{ mK}$ can be analyzed accounting for the constraints imposed on the entropy by the Nernst postulate (third law of thermodynamics) [25]. For such a purpose we compare in Fig. 8 the temperature dependence of the specific heat with the entropy. In the double logarithmic representation of the latter one may appreciate that $C_m(T > T^*)/T$ increases obeying a power law dependence $\propto 1.25/(T^{1.4} + 0.04) \text{ J/mol K}^2$ which, below $T^* = 210 \text{ mK}$, transforms into a 'plateau' with $C_m/T|_{T \rightarrow 0} \approx 7.5 \text{ J/mol K}^2$. The power law dependence, 'plateau' and T^* values are similar to those reported for $\text{YbCu}_{4.3}\text{Au}_{0.7}$ [1].

The area marked as S_m in Fig. 8 represents the entropy computed from the measured specific heat that corresponds to the actual entropy released by the system upon cooling. On the other hand, the area indicated as S_{fit} is extracted as $S_{fit} = \int C_{fit}/T \times dT$, where $C_{fit}/T = 25/(T^{1.4} + 0.04) \text{ J/mol K}^2$ is the fitted power law dependence above $T = T^*$. As a mathematical function, C_{fit}/T keeps growing below T^* as depicted in the figure and therefore the associated entropy exceeds the physical limit of 'Rln 2' for a doublet GS. Both, S_m and S_{fit} entropy trajectories are compared in the figure (right axis). Since the maximum entropy for a doublet GS is $R \ln 2$, the S_{fit} trajectory (continuous curve) is drawn in Fig. 8 taking that value as the high temperature limit. As expected, S_{fit} and S_m coincide within the fitting range (i.e. above T^*), with the $S_m(T)$ for $T > 10 \text{ K}$ being due to the onset of the excited CEF levels contribution. On the low

temperature side, both entropy trajectories also split but due to different reasons. Since the physical system obeys the Nernst principle: $S|_{T \rightarrow 0} \geq 0$, $S_m(T)$ is constrained to change its trajectory and to point to $S_m = 0$ at $T = 0$. Otherwise it would become zero as S_{fit} does at finite temperature (≈ 100 mK in this case). Since that change of trajectory is compelled by thermodynamic principles, T^* characterizes the temperature at which this sort of 'entropy bottleneck' occurs [7].

V. SUMMARY

Based on the parent compound YbCu_5 , we have replaced one Cu atom by Ni to obtain the stoichiometric and atomically well-ordered compound YbCu_4Ni with a lattice parameter $a = 6.9429 \text{ \AA}$ in its cubic structure. At high temperature this compound exhibits localized magnetic nature and an effective magnetic moment close to Yb^{3+} according to the Hund's eight-fold GS. The CEF splits the $J=7/2$ multiplet into well defined doublets as GS and first excited state while the expected quadruplet exhibits a moderate broadening.

At low temperature, this compounds shows clear signs of magnetic frustration reflected in a power law increase of the specific heat by decreasing temperature. This diverging tendency is limited by the Nernst postulate that compels to a change of regime, at a

characteristic temperature $T^* \approx 200$ mK, which in this case corresponds to a 'plateau' with very high density of states: $C_m/T|_{T \rightarrow 0} = 7.5 \text{ J/molK}^2$. Electrical resistivity results confirm this behavior undergoing a broad maximum around 300 mK before to flatten as $T \rightarrow 0$. Both features point to the formation of a Fermi-liquid like GS which does not condensate in a continuous way as is the case in standard Fermi liquids. This feature is highlighted by a maximum in the inductive component of ac-susceptibility at $T \approx T^*$ and a step in the dissipative component.

Although such a large value of $C_m/T|_{T \rightarrow 0}$ was observed in other very heavy fermion compounds after a change of regime from a power law $C_m(T)/T$ increase, the discontinuity observed in the dissipative component of the ac-susceptibility proves that a change of regime occurs at $T = T^*$ in a continuous drift from a frustrated GS to a Fermi-liquid one. Applied magnetic field induces a Zeeman splitting of the doublet ground state, which progressively tends to a Schottky type anomaly in the specific heat as the field overcomes the intensity of the ground state interaction producing the $C_m/T|_{T \rightarrow 0}$ 'plateau'.

ACKNOWLEDGEMENTS

MR and IC are partially supported by projects VEGA 1/0956/17 and VEGA 1/0611/18. AMS thanks the SA-NRF (93549) and the UJ URC/FRC for financial assistance.

-
- [1] I. Curlik, M. Giovannini, J.G. Sereni, M. Zapotokova, S. Gabani, M. Reiffers, *Extremely high density of magnetic excitations at $T = 0$ in $\text{YbCu}_{5-x}\text{Au}_x$* , Phys. Rev. B **90** 224409 (2014).
 - [2] H.v. Löhneysen, A. Rosch, M. Vojta, P. Wölfe, in *Fermi-liquid instabilities at magnetic quantum transitions*, Rev. Mod. Phys. **79** (2007) 1015.
 - [3] G.R. Stewart, in *Non-Fermi-liquid behavior in d- and f-electron metals*, Rev. Mod. Phys. **73** (2001) 797.
 - [4] J.G. Sereni, in *Entropy constraints in the ground state formation of magnetically frustrated systems*, J. Low Temp. Phys. **190** (2018) 1-19, and references therein.
 - [5] T. Gruner, D. Jang, A. Steppke, M. Brando, F. Ritter, C. Krellner, C. Geibel, in *Unusual weak magnetic exchange in YbPt_2Sn and YbPt_2In* , J. Phys.: Condens. Matter **26** 485002 (2014).
 - [6] R. Moessner and A.P. Ramirez, in *Geometrical Frustration*; Physics Today, February 2006, p.24.
 - [7] J.G. Sereni, in *Entropy Bottlenecks at $T \rightarrow 0$ in Ce-Lattice and Related Compounds*, J Low Temp Phys **179** (2015) 126137.
 - [8] A. Yatskar, W.P. Beyermann, R. Movshovich, P.C. Canfield ; Phys. Rev. Lett. **77** (1996) 3637.
 - [9] P. Carretta, R. Pasero, M. Giovannini, C. Baines, Phys.Rev.B, **79**, R020401 (2009).
 - [10] D. Jang, T. Gruner, A. Steppke, K. Mistsumoto, C. Geibel, M. Brando, in *Large magnetocaloric effect and adiabatic demagnetization refrigeration with YbPt_2Sn* , Nature Communications, ncomms9680 (2015).
 - [11] Y. Tokiwa, B. Piening, H.S. Jeevan, S.L. Budko, P.C. Canfield, P. Gegenwart, in *Super-heavy electron material as metallic refrigerant for adiabatic demagnetization cooling*, Sci. Adv. **2** (2016) e1600835.
 - [12] M.S. Torikachvili, S. Jia, E.D. Mun, S.T. Hannahs, R.C. Black, W.K. Neils, D. Martien, S.L. Bud'ko, P.C. Canfield, in *Six closely related related $\text{YbT}_2\text{Zn}_{20}$ heavy fermion compounds with large local moment degeneracy*, PNAS **104** (2007) 9960.
 - [13] Z. Fisk, P.C. Canfield, W.P. Beyermann, J.D. Thompson, M.F. Hundley, H.R. Ott, E. Felder, M. B. Maple, M.A. Lopez de la Torre, P. Visani, C. L. Seamanet; . Phys. Rev. Lett. **67** (1991) 3310.
 - [14] M. Galli, E. Bauer, St. Berger, Ch. Dusek, M. Della Mea, H. Michor, D. Kaczorowski, E.W. Scheidt, F. Marabelli, in *Evolution of ground state properties of $\text{YbCu}_{5-x}\text{Au}_x$* , Physica B **312** & **313** (2002) 489491.

- [15] M. Giovannini, I. Crlk, F. Gastaldo, M. Reiffers, J.G. Sereni, *The role of crystal chemistry in $YbCu_{5-x}Au_x$* , Journal of Alloys and Compounds **627** (2015) 2024.
- [16] J. Rodriguez-Carvajal, Physica B **192** (1993) 55.
- [17] I. Curlik, M. Reiffers, M. Giovannini, in *Study of Magnetic contribution to the Heat Capacity of $YbCu_4Ni$* , Acta Phys. Pol. A **122** (2012) 3-5.
- [18] I. Curlik, S. Matosova, S. Ilkovic, M. Reiffers, M. Giovannini, in *Transport and Magnetic Properties of $YbCu_4Ni$* , Acta Phys. Pol. A **122** (2012) 6-8.
- [19] J.G. Sereni, in *Crystal Field Effects in Metals and Alloys*, Ed. A. Furrer, Plenum Press, N.Y., 1977, 309.
- [20] H.U. Desgrages, K.D. Schotte, in *Specific heat of the Kondo model*, Phys. Lett. A **91** (1982) 240.
- [21] M.B. Maple, in *Superconductivity: a probe for the magnetic state of local moments in metals*, Appl. Phys. **9** (1976) 179-204.
- [22] W.E. Lea, M.J.M. Leask, W.P. Wolf, *The raising of angular momentum degeneracy of f-electron terms by cubic crystal fields*, J. Phys. Chem. Solids **23** (1962) 1381-1405.
- [23] T. Klimczuk, C.H. Wang, J.M. Lawrence, Q. Xu, T. Durakiewicz, F. Ronning, A. Llobet, F. Trouw, N. Kurita, Y. Tokiwa, Han-oh Lee, C.H. Booth, J.S. Gardner, E. D. Bauer, J.J. Joyce, H.W. Zandbergen, R. Movshovich, R.J. Cava, J.D. Thompson, in *Crystal fields, disorder, and antiferromagnetic short-range order in $Yb_{0.24}Sn_{0.76}Ru$* , Phys. Rev. B **84** (2011) 075152.
- [24] J.G. Sereni, in: *Magnetic Systems: Specific Heat*, Saleem Hashmi (editor-in-chief), Materials Science and Materials Engineering. Oxford: Elsevier; 2016. pp. 1-13; ISBN: 978-0-12-803581-8
- [25] A.B. Pippard, in *Elements of classical Thermodynamics*, University Press, Cambridge, 1964.